Author version: Journal of Geophysical Research, vol.113; C11001, 10pp.

Observational evidence for remote forcing of the West India Coastal Current

S. R. Shetye, I. Suresh, D. Shankar, D. Sundar, S. Jayakumar, P. Mehra,
R. G. Prabhudesai, and P. S. Pednekar

National Institute of Oceanography (Council of Scientific and Industrial Research), Goa, India.

Abstract. Circulation in the north Indian Ocean is influenced by both local and remote wind forcing. So far, however, determining the contribution of these two forcing mechanisms at a location has been possible only in numerical experiments. Here, we separate remote and local forcing in observations. Using field measurements (current, sea level, and wind) for a month during March–April 2003 off Goa in the near-coast regime of the West India Coastal Current (WICC), we show that the current was driven by local winds only at periods less than $\sim$ 10 days, with remote forcing contributing at longer periods. The high-passed (HP; period less than 10 days) component of the along-shore current was strongly correlated with the HP component of the along-shore wind, the current lagging the wind by half a day. The low-passed (LP) components of the wind and current were not correlated: the former was unidirectional, but the latter reversed during the period of observation. The relationship between the HP wind and current was used to estimate the locally forced LP current, permitting an estimate of the remote current, the LP residual. This separation of locally- and remotely-forced currents showed that remote forcing contributed as much as local forcing to the WICC. The local current behaved like a classical eastern-boundary current forced by local winds. The reversal in the remote current was due to winds 700 km farther south along the coast; frictional damping had an impact only at periods less than 10 days, there being no remotely forced HP current.

1. Introduction

The north Indian Ocean (north of $\sim 10^\circ$S) has three special features. First, it is purely tropical, being confined south of $\sim 25^\circ$N by the Asian landmass. Circulation in the region is therefore dominated by features that are peculiar to the tropics, such as equatorially-trapped waves. Second, the north Indian Ocean comes under the influence of winds that are known for their variability with time. The best known are the monsoon winds with a distinct annual cycle. Superimposed on the seasonal cycle are variations with periods from a few days to a few months, including bi-weekly oscillations [*Krishnamurti and Bhalme*, 1976] and Madden-Julian oscillations [*Madden and Julian*, 1971, 1972]. Third, the basin is small. Its equatorial stretch is only $\sim$ 7000 km compared to $\sim$ 20000 km of the Pacific. This small size has two implications. First, the area that comes under the influence of coastally trapped waves (coastal Kelvin waves, edge waves, etc.) forms a significant fraction of the total area of the basin. Second, there is wide scope for interaction between coastally-trapped and equatorially-trapped waves. These special features together imply that circulation in the basin is dominated by equatorially- and coastally-trapped waves, and there exist winds to trigger these waves.

The presence of the above waves means that circulation at any location consists of locally-forced motions and motions that are a consequence of arrival of waves generated elsewhere. Specifically, at a coastal location, *local* forcing means the direct effect of the along-shore component of the coastal winds, with all other effects being classified as *remote* forcing [*Schott and McCreary*, 2001]. The importance of remote forcing (in the Indian Ocean) was first pointed out by *Lighhill* [1969]: he showed that long, baroclinic waves travel much faster in the vicinity of the equator, leading to the Somali Current reversing direction shortly after the winds reverse direction over the north Indian Ocean. Later work focussed on the Somali Current and the equatorial currents in the Indian Ocean [see the review in *Schott and McCreary*, 2001, for more details]. Application of this idea to the Bay of Bengal was first due to *Potemra et al.* [1991] and *Yu et al.* [1991]. In a comprehensive model study of the entire Indian Ocean, *McCreary et al.* [1993] emphasised the importance of remote forcing for the circulation in the north Indian Ocean. A number of studies since then have emphasized the importance of local and remote forcing for the circulation in the Bay of Bengal [*Shankar et al.*, 1996; *McCreary et al.*, 1996; *Vinayachandran et al.*, 1996; *Rao et al.*, 2002; *Han and Webster*, 2002] and the Arabian Sea [*Bruce et al.*, 1994; *Shankar and Shetye*, 1997; *Bruce et al.*, 1998; *Shenoi et al.*, 2004]. A detailed examination of the mechanisms forcing the seasonally reversing, trans-basin monsoon currents in the open ocean was presented in *Shankar et al.* [2002].

All the above studies are primarily numerical experiments that make a case for the important role of remote forcing in the circulation observed in the north Indian Ocean. While this is useful, it is important to analyse observed currents, and to identify in them the components that can be linked to local and remote forcing without having to resort to numerical model simulations. Separation between locally and remotely forced currents using observations is the objective of this paper. We use data collected off Goa on the Indian west coast to show that, during the period of observations, the West India Coastal Current (WICC) [*Shankar*

and Shetye, 1997] was forced both remotely and locally at periods exceeding 10 days; at periods less than 10 days, the WICC was locally forced.

The next section describes the data used; Section 3 describes the relationship between sea level, current, and wind, Section 4 describes the method of analysis for estimating the high-frequency or high-passed component of the current, Section 5 describes the method of estimating the remotely forced component of the current, and Section 6 concludes the paper.

2. Data

Data on currents, sea level, and winds were collected off Goa on the Indian west coast (see Figure 1) for a month during March–April 2003 under a programme on Integrated Coastal and Marine Area Management (ICMAM). Currents were measured using current meters (Aanderaa make, self-recording) at five locations (see Table 1) on the inner shelf within the 20 m isobath. Winds were measured using an automatic weather station located on the terrace of the National Institute of Oceanography (Figure 1 and Table 1). Sea level was measured using a Valeport pressure-sensor tide gauge at Verem near the mouth of the Mandovi estuary (Figure 1 and Table 1).

The current meters were located at "mid-depth" in the water column: the water-column depths at the five current-meter locations are given in Table 1. The currents were measured at an interval of 10 minutes. The current data were first de-tided using the software TASK (Tidal Analysis Software Kit) [*Bell et al.*, 1998]. The de-tided (residual) current components (zonal and meridional) were then rotated to yield the along-shore and cross-shore components. The rotation angle was estimated by minimising the cross-shore component in the least-squares sense: the assumption here was that the non-tidal component of the current would be largely along-shore. The along-shore components of the residual at the five locations was visually coherent (Figure 2), implying a common forcing mechanism; the cross correlations of the along-shore components were also significant at the 99% level (Table 2).

The winds were measured at an interval of 10 minutes on the terrace of the National Institute of Oceanography in Dona Paula (see Figure 1). An earlier study [*Aparna et al.*, 2005] has shown that these anemometer winds are significantly correlated with the winds measured by the QuikSCAT scatterometer; the QuikSCAT winds are estimated at the standard height of 10 m. Prominent in the wind record for March–April is the sea breeze, as seen in typical [*Aparna et al.*, 2005] and average hodographs [*Neetu et al.*, 2006] for the period. The wind speed and direction were used to compute the cross-shore and along-shore components; this decomposition was done using the average angle of orientation of the coast in the vicinity of the anemometer. The along-shore component of the wind is shown in Figure 3; also plotted is the along-shore wind decimated with a 0.75 day^{-1} ($\sim$ 32 hours) filter to remove the sea-breeze cycle.

During the ICMAM observations, sea level was measured using tide poles at 13 locations within the Mandovi and Zuari estuaries and the Cumbarjua canal connecting them. These tide-pole data, collected at an interval of 15 minutes, were described in detail by *Sundar and Shetye* [2005], who noted that the accuracy of the tide-pole data was good enough to separate 34 tidal constituents. At Verem, which is located nearest the mouth of the Mandovi estuary (Figure 1) and is therefore most representative of the coastal sea level, a pressure-sensor tide gauge was deployed in addition to the tide pole. The tide-pole data were noisier, but there was good agreement between the tide-pole and pressure-sensor data. We use the pressure-sensor data in this paper because these data are the most representative of the sea level at the coast. The sea level was also de-tided using TASK [*Bell et al.*, 1998]; the de-tided, or residual, sea level is shown in Figure 3. Superimposed on the residual is the residual sea level after application of the 0.75 day^{-1} low-pass filter; a second order Butterworth filter, implemented in MATLAB, was used. This filter reduces considerably the noise in the sea-level record.

Though we analysed all five current-meter records, we picked the 20 m record at Colva (location C20 in Figure 1) for comparison with the wind and Verem sea level. The along-shore current at C20 is plotted in Figure 3 along with the along-shore current filtered with the 0.75 day^{-1} low-pass filter.

In the rest of this paper, we use only the data filtered with the 0.75 day^{-1} low-pass filter. Hence, hereafter, "wind" implies the 0.75 day^{-1}-filtered along-shore wind, "sea level" implies the de-tided and 0.75 day^{-1}-filtered sea level, and "current" implies the de-tided and 0.75 day^{-1}-filtered along-shore current.

3. Coastal sea level and along-shore current

The sea-level record was noisier than the current or wind records (Figure 3). Most prominent in a smoothed periodogram [*Emery and Thomson*, 1998] of the sea level was an oscillation with a period of $\sim$ 3.6–5.7 days (Figure 3). The 3.6-day period was also evident in the C20 current-meter record, but the currents also showed a peak around $\sim$ 14 days. Sea level and current were significantly correlated (Table 2), suggesting that a quasi-geostrophic balance probably holds even at this short period. The wind spectrum peaked at $\sim$ 5.7 days, but the energy dropped at lower frequencies; the wind, however, was less well correlated with current and sea level (Table 2). (The spectra for the other four current meters, shown in Figure S1, were similar to that for the C20 current meter.) The same periodicities are seen in a wavelet analysis [*Torrence and Compo*, 1998] of the data (Figure S2), but the wavelet time series also shows that there is considerable variation in the energy at a given period even within the short duration of the measurements. The short record length, however, makes it difficult to draw more inferences from the spectra. It leads to a large error bar for the estimated periodograms (Figure 3) and the cone of influence of the wavelet power spectra limits the interpretable part of the spectra to periodicities less than 10 days.

The possibility of a quasi-geostrophic balance and the coherence of the five current-meter records (Figure 2) suggest that large-scale dynamics are important even at such shallow depths on the continental shelf. The question then is the following. Are the observed currents in this near-shelf regime forced only by local winds, the coherence and correlation among the current meters (Figure 2 and Table 2) arising as a consequence of large-scale coherence in the winds (*Aparna et al.* [2005] suggest that there is considerable along-shore coherence even in the sea breeze off the Indian west coast.), or is remote forcing also important?

The numerical model studies referred to earlier were primarily concerned with the seasonal cycle and usually used monthly-mean data (winds, sea level, currents, etc.) for forcing (the model ocean) and validation. These studies suggest that forcing by winds remote from the location of current measurement is an important, and often dominant, cause of the observed seasonal cycle of the WICC [*Schott and McCreary*, 2001]; for example, the seasonal cycle of the Lakshadweep high in the southeastern Arabian Sea is forced primarily by the winds that blow along the east coast of India [*McCreary et al.*, 1993; *Shankar and Shetye*, 1997;

Shankar et al., 2002]. Is remote forcing still important for the WICC at the short periods that can be resolved by the one-month records described above? Is remote forcing important even in the shallow depths of the near-coastal shelf regime? Though some model studies [*Bruce et al.*, 1998; *Nethery and Shankar*, 2007; *Kurian and Vinayachandran*, 2007] suggest that remote forcing is important for the WICC even at intra-seasonal periods, most of the numerical model studies referred to earlier were primarily concerned with the large-scale WICC that is trapped against the continental slope [*Shetye et al.*, 1990, 1991]. The analysis presented in the following section aims at separating the effects of local and remote forcing in the shallow current-meter observations on the continental shelf.

4. High-passed current

4.1. Observed high-passed current

A relationship between the local wind and current was not as obvious as between sea level and current (Figure 3). Hence, we filtered both wind and current with a low-pass filter; as with the 0.75 day^{-1} low-pass filter used earlier, this filtering was also done using a second order Butterworth filter. The filter cutoff period was varied between 5–20 days and the high-passed (HP) wind and current were obtained by subtracting the resultant of the filter operation, which yielded the low-passed (LP) wind and current (for the given filter cutoff period), from the wind and current. (Note that the wind and current subjected to this low-pass filter were the wind and current that were the result of the earlier filtering with the 0.75 day^{-1} low-pass filter. The tide and the diurnal cycle had been eliminated *a priori* from the data subjected to the 0.75 day^{-1} low-pass filter.)

We then computed the lagged correlation between the HP wind and HP current (current lagging wind) for all five current meters. The correlation between the HP wind and HP current was maximum for a filter cutoff period of ~ 10 days; the correlation between the LP wind and LP current was minimum around the same filter cutoff period (Figure 4 and Figure S3). This extremum in correlation (whether maximum or minimum) was obvious for the current meters off Colva and Mormugao; for the current meters off Arambol, the HP correlation maximum occurred at 12 days, but the correlation between the LP wind and LP current did not exhibit a minimum (Figure S3).

10 days turned out to be the shortest period for which we could separate the HP and LP components for the five current meters; hence, a low-pass filter of cutoff period ~ 10 days was used to separate the HP component of the wind and current from the LP component. The key result of this paper, that remote forcing is important for the WICC at periods greater than 10 days, does not depend on this choice of filter cutoff period. Apart from this filter cutoff period, this filtering operation also yielded a lag (say $l_{\max}$) at which the correlation was maximum for each current meter. We call these HP and LP components the *observed* HP and LP components of the wind and current because the only operation carried out on the (de-tided and filtered with the 0.75 day^{-1} filter) wind and current data was the application of the 10-day low-pass filter.

4.2. Estimated high-passed current

There was a striking visual coherence between the HP wind and current, with the current lagging the wind (Figure 5a and panel (a) in Figures S4–S8). The visual coherence between the HP wind and current implies that the current can be derived as a linear function of the wind. We tested this hypothesis by looking for a relation of the form

$$c(i) = Aw(i + l), \qquad (1)$$

where $c(i)$ is the current at time i (i is an index for time), $w(i)$ is the wind, A is a scale or amplification factor, and l is a positive lag; like i, l is a positive integer, and an increment of 1 in both implies a time increment of 10 minutes. In Equation (1), the current is in cm s^{-1} and the wind is in m s^{-1}; the conversion of units is accounted for in A. The current estimated by applying this relation to the HP wind is called the *estimated* HP current.

This computation was carried out for all five current meters for $0.025 \leq A \leq 0.155$ and $l = [l_{\max} - 10, l_{\max} + 10]$. (The lag index l was varied around the $l_{\max}$ obtained earlier for each current meter.) The optimum values of A and l were obtained in a least-squares sense by minimising the deviation of the estimated current from the observed HP current. The correlations between the estimated and observed HP currents are listed in Table 3; these correlations were significant at the 99% level. Note that this estimated HP current is determined purely from the local wind. The observed and estimated HP current for current meter C20 are shown in Figure 5c; see panel (c) of Figures S4–S7 for the other four current meters and of Figure S8 for a colour version of Figure 5c.

5. Low-passed current

5.1. Separation of locally and remotely forced components

Unlike with the HP wind and current, no relationship was apparent between the LP wind and current: the LP wind was unidirectional, but the LP current changed direction during the month (Figure 5b and panel (b) in Figures S4–S8). We assumed that the relationship derived (using Equation 1) between the HP wind and current would hold at lower frequencies too. In other words, we assumed that the LP component of the local wind would force a LP current, and that the scale factor and lag derived for the HP component would also apply to the LP component. Applying Equation (1) to the LP wind then yielded the *estimated* LP *local* current. The difference between the (observed) LP current (Figure 5b) and its estimated local component was therefore the *remotely* forced component. The locally and remotely forced LP current components are shown in Figure 5d. Like the LP wind, the locally forced LP current was unidirectional during the month; it is the remotely forced current that was responsible for the change in direction of the LP current.

Thus, the wind and current data from the Indian west coast show that the de-tided along-shore current off Goa on the Indian west coast (the WICC) can be separated into a locally forced part that consists of both HP and LP components and a LP remotely forced part (Figure 5e). The HP (LP) component in this separation had a period less (greater) than 10 days.

The sum of the locally and remotely forced components yielded the total estimated current. It is plotted along with the observed current in Figure 5f. The correlations between the total estimated current and the observed current for the five current meters are listed in Table 3; all the correlations were significant at the 99% level.

5.2. Remote forcing of the WICC

What is striking is that remote forcing seems to be important even at periods as short as 10 days and in the immediate vicinity of the coast. The earlier model studies [*McCreary et al.*, 1993; *Bruce et al.*, 1994; *Shankar and Shetye*, 1997; *Shankar et al.*, 2002] had dealt only with the seasonal cycle and did not resolve the inner shelf; many of these studies

used models of the reduced-gravity class and therefore had a vertical wall for the coast. The observations reported here, on the contrary, were made in the near-coastal regime of the continental shelf in very shallow waters (water depth less than 20 m). Hence, our results imply that remote forcing via the medium of shelf or edge waves has a significant impact on the current even in the vicinity of the coast.

Since these waves propagate with the coast on their right (in the northern hemisphere) at the sub-inertial periods of interest to us, they must be forced by winds farther south along the coast, or, as in the seasonal-cycle model simulations, by the winds blowing along the Indian east coast [*McCreary et al.*, 1993; *Bruce et al.*, 1994; *Shankar and Shetye*, 1997; *Bruce et al.*, 1998; *Shankar et al.*, 2002]. But one question remains: what is the source of this remote forcing? How far "upstream" can we trace the waves that must be contributing to the current off Goa?

We used QuikSCAT wind data to determine the possible source of the remote forcing. As has been shown earlier [*Aparna et al.*, 2005], the vector correlation between the anemometer wind and QuikSCAT wind is significant; both yield the same direction for the wind, but the QuikSCAT wind has a higher magnitude. Though the QuikSCAT winds have a poorer temporal resolution (nominally three days, though the data were optimally interpolated to a daily resolution in the wind product we used) than the anemometer winds (every 10 minutes), we subjected both data sets to the same 10-day filter. The HP QuikSCAT wind was comparable to the HP anemometer wind (Figure 6a) and the two had roughly similar magnitudes. The LP QuikSCAT component was, however, much stronger than its LP anemometer component (Figure 6b), implying that the stronger QuikSCAT signal reported in *Aparna et al.* [2005] is due more to the LP component.

A time-latitude plot of the LP along-shore component of the QuikSCAT wind (Figure 6d) suggests that the poleward along-shore LP current could *not* have been forced by the winds north of $\sim 9^{\circ}$N: the wind is poleward only south of this latitude. Hence, the poleward remotely forced component of the current off Goa (Figure 6c) was forced during March from at least as far south as Kollam (see Figure 1), just north of the southern tip of India. The source of the remote forcing for the current reversal off Goa was ~ 700 km south of the current-meter locations. The second time the poleward current was seen was in mid-April, but the poleward wind was seen only farther south, at $\sim 8^{\circ}$N, which is the location of the southern tip of India. Hence, it is possible that the second reversal in April was forced either from the Gulf of Mannar or from the Bay of Bengal. Tracing the source of the current reversal any farther, however, is beyond the scope of this paper.

5.3. Aliasing of the error to the remote signal

We note here one caveat of the method. Note the spread between the remotely forced component of the current at the five current meters (Figure 7). Given the distance over which this remote forcing acts (~ 700 km), it is inconceivable that the difference between the remotely forced component at the five current-meter locations (the distance between the current meters off Arambol and Colva is less than one Rossby radius), could be as much as the difference between the locally forced components (Figure 7). The problem lies in the sparsity of wind data and the method used. With just one anemometer available to estimate the HP locally forced current (using Equation 1), the difference between the locally forced component at the five locations is underestimated, and this error is transferred to the LP remotely forced component, which is estimated as a residual. The QuikSCAT data show that there is considerable along-shore variation in the along-shore wind, the difference between the winds at $\sim 15^{\circ}$N and $\sim 16^{\circ}$N exceeding 1 m s^{-1} at times. This along-shore variation is most likely the reason for the difference between the observed HP components of the current at the five current meters (Figure S9) and for the strikingly different wind-current correlations between Arambol and Colva (Figure S3). Hence, notwithstanding the along-shore coherence documented in the wind observed off the Indian west coast [*Aparna et al.*, 2005], the along-shore variations are sufficient to force a measureable difference between the locally forced current even within one Rossby radius. This measurable difference in the locally forced component is aliased by the sparse wind data and method into the remotely forced component of the current.

6. Discussion

Nevertheless, the key result of the paper is robust. There is a reversal in the LP current off Goa during the period of observations, but there is no such reversal in the LP wind off Goa; the QuikSCAT wind data unequivocally support this observation. The reversal in the current is therefore due to remote forcing and the QuikSCAT winds suggest that the required reversal in the wind does not occur equatorward along the coast till off Kollam ($\sim 9^{\circ}$N). Thus, the wind and current data from the inner continental shelf off Goa on the Indian west coast show that even at depths as shallow as 20 m, remote forcing makes a significant contribution to the WICC. Hence, the WICC is forced both locally and remotely at periods exceeding 10 days; at periods less than 10 days, it is locally forced.

The wind data from QuikSCAT suggest that the reversal in the observed current off Goa was forced by winds just north of the southern tip of India (Figure 6). The distance between this poleward wind forcing and the current meters is around 700 km, over half the length of the Indian west coast. Off the continental shelf, on the continental slope where the core of the WICC is trapped [*Shetye et al.*, 1990, 1991], the analytic study of *Nethery and Shankar* [2007] showed that at a period of 30 days, the energy associated with the coastal Kelvin wave propagates down (upward phase propagation) as the wave propagates poleward along the continental slope off the Indian west coast. This downward energy propagation can be visualised as a (Kelvin) beam that bends down as the wave propagates: the downward bending at a period of 30 days was estimated by *Nethery and Shankar* [2007] to be ~ 200 m over the distance between Kollam and the current meters off Goa (Figure 1). The energy put in by the wind at the surface near the southern tip of India would therefore force a current at greater depths as the wave propagated poleward, while the surface current decorrelates rapidly along the coast. Hence, unlike on the continental shelf, at the periods resolved by the data used here, the winds blowing off southwest India cannot force similar changes in the surface current on the continental slope off Goa: the effect of remote forcing from the Bay of Bengal is unlikely to be felt beyond the regime of the Lakshadweep High [*Bruce et al.*, 1994; *Shankar and Shetye*, 1997], where remote forcing from the bay has been shown to be important at intra-seasonal periods [*Bruce et al.*, 1998; *Kurian and Vinayachandran*, 2007]. In other words, the reversal seen in the current on the shelf off Goa may not be accompanied by a similar surface-current reversal on the slope.

On the continental shelf, the Kelvin wave (which propagates along a vertical wall like the continental slope) is replaced by the shelf or edge wave (which are affected by the bottom topography of the shelf), which cannot bend in a similar fashion. It is remarkable, however, that the higher friction, which must act to dissipate these waves in the shallow depth regimes investigated here, does not damp out the remotely forced signal even over a distance of ~ 700 km. It

is only when the period decreases below 10 days that the effect of friction (bottom friction, horizontal or Laplacian friction, and mixing due to interaction with the tides) dominates, resulting in the high correlation observed between the local wind and local current. The frictional damping ensures that the remotely forced component is negligible at periods shorter than 10 days, permitting a linear relation between the wind and current. This linear relation, inferred for the HP component of the wind and current, was assumed to hold for the locally forced LP component too, the sum of these two locally forced components yielding the net locally forced current.

Thus, the local component of the WICC behaved like a classical, eastern-boundary current forced by local winds, the current lagging the wind by about half a day (Table 3). Though it is difficult to draw an inference from just two current meters, there was a tendency off both Arambol and Colva for the scale factor A (see Equation 1) to decrease offshore (from 10 m to 20 m depth) (Table 3), pointing to the decreasing efficiency with which the wind couples to the ocean as depth increases. This response is typical of a locally forced eastern-boundary current. The sea-level response was slower, with the sea level at the coast taking almost a day more than the current to respond to the wind (Figure 3 and Table 2). The inertial period at $\sim 15.5°$N is 45 hours; hence, the purely local response of both current and sea level occurred within an inertial period.

The remotely forced component consisted of periodicities exceeding 10 days, which is ~ 5.3 times the local inertial period. Spectral analysis (Figures 3 and S2) showed that the energy of the periodogram or the power of the wavelet was comparable at periods less than and greater than 10 days, but the short records make it difficult to draw conclusive inferences from the spectra alone. The analysis reported here shows, however, that the remotely forced component was comparable to the locally forced component: both had a range of ~ 20 cm s^{-1}. Hence, even in order to simulate the WICC on the continental shelf in the vicinity of the Indian west coast, it is necessary to model a domain that extends beyond the immediate region of interest. The wind-forcing regime for the currents off Goa extends at least into the Gulf of Mannar, and the intra-seasonal (periodicities greater than 10 days) WICC at the shallow depths sampled here may even be influenced by winds blowing along the Indian east coast, as is the seasonal WICC on the continental slope off Goa [*McCreary et al.*, 1993; *Shankar and Shetye*, 1997].

This role of remote forcing had been highlighted by earlier model studies, which showed that it was necessary to invoke remote forcing to simulate the seasonal cycle of the WICC, but confirmation in observations was lacking. This is the first demonstration in observations of the importance of remote forcing for the WICC.

Acknowledgments. The observations reported in this paper were made during a project on Integrated Coastal and Marine Area Management (ICMAM); the observational programme was funded by ICMAM, Chennai. This research has been supported by the Council of Scientific and Industrial Research (CSIR), New Delhi and the Indian National Centre for Ocean Information Services (INCOIS), Hyderabad. The tide-pole data were collected by INDOMER Coastal Hydraulics (P) Ltd., Chennai. The QuikSCAT wind data were downloaded from `http://www.ssmi.com`. The MATLAB code for wavelet analysis [*Torrence and Compo*, 1998] was downloaded from `http://paos.colorado.edu/research/wavelets` and the MATLAB code for the periodogram (developed by Alejandro Sanchez of the US Army Corps of Engineers) from `http://www.mathworks.com/matlabcentral/`. Critical comments from S. S. C. Shenoi and Daniel Nethery and from two anonymous reviewers helped improve the manuscript: the spectral analysis was done in response to a comment from the reviewers. K. Suprit helped with Figure 1. This is NIO contribution 4418.

References

Aparna, M., S. R. Shetye, D. Shankar, S. S. C. Shenoi, P. Mehra, and R. G. P. Desai, Estimating the seaward extent of sea breeze from QuikSCAT scatterometry, *Geophys. Res. Lett.*, *32*, L13601, doi:10.1029/2005GL023107, 2005.

Bell, C., J. M. Vassie, and P. L. Woodworth, *POL-PSMSL Tidal Analysis Software Kit 2000 (TASK-2000)*, Permanent Service for Mean Sea Level, Proudman Oceanographic Laboratory, UK, 1998.

Bruce, J. G., D. R. Johnson, and J. C. Kindle, Evidence for eddy formation in the eastern Arabian Sea during the northeast monsoon, *J. Geophys. Res.*, *99*, 7651–7664, 1994.

Bruce, J. G., J. C. Kindle, L. H. Kantha, J. L. Kerling, and J. F. Bailey, Recent observations and modeling in the Arabian Sea Laccadive High region, *J. Geophys. Res.*, *103*, 7593–7600, 1998.

Emery, W. J., and R. E. Thomson, *Data analysis methods in physical oceanography*, Pergamon Elsevier Science, London, U. K., 1998.

Han, W., and P. J. Webster, Forcing mechanisms of sea level interannual variability in the Bay of Bengal, *J. Phys. Oceanogr.*, *32*, 216–239, 2002.

Krishnamurti, T. N., and H. N. Bhalme, Oscillations of a monsoon system, Part I: Observational aspect, *J. Atmos. Sci.*, *33*, 1937–1954, 1976.

Kurian, J., and P. N. Vinayachandran, Mechanisms of formation of the Arabian Sea mini warm pool in a high-resolution ocean general circulation model, *J. Geophys. Res.*, *112*, C05009, doi:10.1029/2006JC003631, 2007.

Lighthill, M. J., Dynamic response of the Indian Ocean to the onset of the southwest monsoon, *Phil. Trans. R. Soc. Lond.*, *265A*, 45–92, 1969.

Madden, R. A., and P. R. Julian, Description of a 40–50 day oscillation in the zonal wind in the tropical Pacific, *J. Atmos. Sci.*, *28*, 702–708, 1971.

Madden, R. A., and P. R. Julian, Description of global-scale circulation cells in the tropics with a 40–50 day period, *J. Atmos. Sci.*, *29*, 1109–1123, 1972.

McCreary, J. P., P. K. Kundu, and R. L. Molinari, A numerical investigation of the dynamics, thermodynamics and mixed-layer processes in the Indian Ocean, *Prog. Oceanogr.*, *31*, 181–244, 1993.

McCreary, J. P., W. Han, D. Shankar, and S. R. Shetye, Dynamics of the East India Coastal Current, 2. Numerical solutions, *J. Geophys. Res.*, *101*, 13,993–14,010, 1996.

Neetu, S., S. R. Shetye, and P. Chandramohan, Impact of sea breeze on wind-seas off Goa, west coast of India, *J. Earth Syst. Sci.*, *115*, 229–234, 2006.

Nethery, D., and D. Shankar, Vertical propagation of baroclinic Kelvin waves along the west coast of India, *J. Earth Syst. Sci.*, *116*, 331–339, 2007.

Potemra, J. T., M. E. Luther, and J. J. O'Brien, The seasonal circulation of the upper ocean in the Bay of Bengal, *J. Geophys. Res.*, *96*, 12,667–12,683, 1991.

Rao, A. S., V. V. Gopalakrishna, S. R. Shetye, and T. Yamagata, Why were cool SST anomalies absent in the Bay of Bengal during the 1997 Indian Ocean Dipole event?, *Geophys. Res. Lett.*, *29*, 10.1029/2001GL014,645, 2002.

Schott, F. A. and J. P.McCreary, The monsoon circulation of the Indian Ocean, *Prog. Oceanogr.*, *51*, 1–120, 2001.

Shankar, D., and S. R. Shetye, On the dynamics of the Lakshadweep high and low in the southeastern Arabian Sea, *J. Geophys. Res.*, *102*, 12,551–12,562, 1997.

Shankar, D., J. P. McCreary, W. Han, and S. R. Shetye, Dynamics of the East India Coastal Current, 1. Analytic solutions forced by interior Ekman pumping and local alongshore winds, *J. Geophys. Res.*, *101*, 13,975–13,991, 1996.

Shankar, D., P. N. Vinayachandran, and A. S. Unnikrishnan, The monsoon currents in the north Indian Ocean, *Prog. Oceanogr.*, *52*, 63–120, 2002.

Shenoi, S. S. C., D. Shankar, and S. R. Shetye, Remote forcing annihilates barrier layer in southeastern Arabian Sea, *Geophys. Res. Lett.*, L05307, doi:10.1029/2003GL019270, 2004.

Shetye, S. R., A. D. Gouveia, S. S. C. Shenoi, D. Sundar, G. S. Michael, A. M. Almeida, and K. Santanam, Hydrography and circulation off the west coast of India during the southwest monsoon 1987, *J. Mar. Res.*, *48*, 359–378, 1990.

Shetye, S. R., A. D. Gouveia, S. S. C. Shenoi, G. S. Michael, D. Sundar, A. M. Almeida, and K. Santanam, The coastal current off western India during the northeast monsoon, *Deep-Sea Res.*, *38*, 1517–1529, 1991.

Sindhu, B., I. Suresh, A. S. Unnikrishnan, N. V. Bhatkar, S. Neetu, and G. S. Michael, Improved bathymetric datasets for the shallow water regions in the indian ocean, *J. Earth Syst. Sci.*, *116*, 261–274, 2007.

Sundar, D., and S. R. Shetye, Tides in the Mandovi and Zuari estuaries, Goa, west coast of India, *J. Earth Syst. Sci.*, *114*, 493–503, 2005.

Torrence, C., and G. P. Compo, A practical guide to wavelet analysis, *Bull. Am. Met. Soc.*, *79*, 61–78, 1998.

Vinayachandran, P. N., S. R. Shetye, D. Sengupta, and S. Gadgil, Forcing mechanisms of the Bay of Bengal circulation, *Curr. Sci.*, *71*, 753–763, 1996.

Yu, L., J. J. O'Brien, and J. Yang, On the remote forcing of the circulation in the Bay of Bengal, *J. Geophys. Res.*, *96*, 20,449–20,454, 1991.

S. R. Shetye, I. Suresh, D. Shankar, D. Sundar, S. Jayakumar, P. Mehra, R. G. Prabhudesai, and P. S. Pednekar, National Institute of Oceanography, Dona Paula, Goa 403004, India. (shankar@nio.org).

Tables

Variable	Station	Latitude	Longitude	D	Data start	Data end
Current	Off Arambol	15°39.41′N	73°41.11′E	10/5.5	14:06, 18 March	09:56, 17 April
Current	Off Arambol	15°37.98′N	73°38.77′E	20/9.5	12:31, 18 March	14:01, 19 April
Current	Off Mormugao	15°23.66′N	73°43.37′E	20/9.5	11:38, 19 March	09:38, 18 April
Current	Off Colva	15°16.63′N	73°53.16′E	10/5.5	10:46, 20 March	10:26, 19 April
Current	Off Colva	15°14.08′N	73°50.93′E	20/9.5	14:09, 19 March	07:39, 19 April
Sea level	Verem	15°30.10′N	73°48.80′E	4.5	17:01, 11 March	11:31, 14 April
Wind	Dona Paula	15°27.38′N	73°48.14′E	48.14	00:00, 1 January	24:00, 31 December

Table 1. Summary of the observations used; all data were collected during March–April 2003. The five current meters (RCM7, Aanderaa self-recording meters) were deployed in a water column of depth D (column 5); the second value listed is the depth of the current meter below the chart datum. For the tide gauge (anemometer), this column lists the depth of the water column (height above mean sea level). The tide gauge was of make Valeport (type: pressure-sensor) and the anemometer was of make R. M. Young (Model 05103). All values in column 5 are in metres; time (columns 6 and 7) is Indian Standard Time (IST), which is 5:30 hours ahead of UTC.

	A10		A20		M20		C10		C20		SL		W	
A10	—	—	0.89	2:50	0.88	0:50	0.83	—	0.81	—	0.68	22:00	0.70	—
A20	0.89	—	—	—	0.94	—	0.76	—	0.88	—	0.60	21:10	0.54	—
M20	0.88	—	0.94	0:30	—	—	0.87	—	0.93	—	0.71	23:20	0.62	—
C10	0.83	2:10	0.76	5:10	0.87	3:10	—	—	0.88	0:10	0.74	26:00	0.71	—
C20	0.81	0:40	0.88	4:00	0.93	2:30	0.88	—	—	—	0.69	25:10	0.54	—
SL	0.68	—	0.60	—	0.71	—	0.74	—	0.69	—	—	—	0.49	—
W	0.70	11:50	0.54	14:10	0.62	14:20	0.71	10:00	0.54	10:40	0.49	33:20	—	—

Table 2. Cross-correlation matrix for the observed variables. A10 (A20) represents the along-shore current at Arambol at 10 m (20 m) water depth, C10 (C20) represents the along-shore current at Colva at 10 m (20 m) water depth, M20 represents the along-shore current at Mormugao, SL represents the sea level at Verem, and W represents the along-shore wind at Dona Paula. The first number in each labelled column gives the correlation and the second number the lag (in hours:minutes). All correlations were significant at the 99% level. The variable listed in the column lags the variable listed in the rows; negative lags are not listed in this matrix. For example, the correlation between A20 and A10 is 0.89 and the former lags the latter by 170 minutes; current meter C10 leads all other current meters and the wind leads the current and sea level. Before computing the correlations, the currents and sea level were de-tided and filtered with a 0.75 day^{-1} ($\sim$ 32 hours) filter, and the wind was filtered with the 0.75 day^{-1} filter.

CM	Scale	Lag	r_{hf}	r_{oe}
A10	0.075	11:40	0.71	0.88
A20	0.055	13:40	0.63	0.89
M20	0.095	14:30	0.73	0.89
C10	0.085	10:50	0.75	0.88
C20	0.045	11:30	0.70	0.90

Table 3. Scale, lag, and correlations for the five current meters. The current meter is identified in column 1; the scale factor c and time lag (hours:minutes) (see Equation (1)) are in columns 2 and 3. Column 4 lists the correlation between the HP wind and HP estimated current. Column 5 lists the correlation between the total (sum of HP and LP (both local and remote components)) observed and estimated currents; this correlation, significant at the 99% level for all five current meters, determines the "goodness" of the estimated current.

Figures

Captions

Figure 1. The location of the observation platforms. (a) The north Indian Ocean. (b) The Indian west coast. The solid lines offshore mark the 50, 100, and 200 m isobath; bathymetry data are based on the $2'$ Indian-Ocean data set of *Sindhu et al.* [2007]. (c) Large-scale map of the study region off Goa. The dotted lines mark the 10 and 20 m isobaths. The current-meter locations are shown by filled circles and are labelled by the first letter of the nearby town and the depth of the water column at the location. Thus, A10 (A20) represents the current meter in 10 m (20 m) water depth off Arambol, M20 the current meter off Mormugao, and C10 (C20) the 10 m (20 m) current meters off Colva. Sea level was measured at Verem using a Valeport tide gauge. The winds were measured using an automatic weather station located on the terrace of the National Institute of Oceanography in Dona Paula. Note that the Mormugao current meter lies offshore of the channel of the Zuari estuary.

Figure 2. Currents measured at A10 (top panel), A20 (second panel), M20 (third panel), C10 (fourth panel), and C20 (bottom panel). The cross-shore (grey) and along-shore (black) components of the de-tided current are plotted. Units are cm s^{-1}. The abscissa gives the time in Julian Day of 2003.

Figure 3. (Left) Along-shore wind (top, m s^{-1}), de-tided sea level (middle, cm), and de-tided along-shore current (bottom, cm s^{-1}) (grey curves). The current plotted is for current meter C20. The black curves superimposed on the wind, de-tided current, and sea level are the wind, current, and sea level filtered with a 0.75 day^{-1} ($\sim$ 32 hours) filter that eliminates the sea breeze and its effect. The abscissa gives the time in Julian Day of 2003. (Right) Smoothed periodograms of the wind (top), sea level (middle), and along-shore current (bottom). Note that both axes are plotted on a logarithmic (base 10) scale. The unit of the abscissa (frequency) is cycles day^{-1} and that of the ordinate (power spectral density or PSD) is X^2 day, where X is the unit of the respective variable in the corresponding left panel. Note that the ordinate of the wind periodogram is scaled by a factor of 100. To compute the periodograms, we applied a 75% Tukey window (cosine taper) to the de-trended (and de-tided) data, and then computed a three-point smoothed periodogram using band averaging as described by *Emery and Thomson* [1998]. The bar in the upper left corner of each panel is the 95% confidence interval.

Figure 4. Correlation between wind and along-shore current as a function of filter cutoff period. The HP (high-passed, filter cutoff period on abscissa) correlation (grey curve, inverted triangles) peaked at around 10 days; the LP (low-passed) correlation (black curve, triangles) was a minimum at around 10 days. Hence, a filter cutoff period of 10 days was used to separate the HP component from the LP component. This figure shows the curves for the C20 current meter; see Figure S3 for the corresponding plots for the other four current meters.

Figure 5. Separation of along-shore current into locally and remotely forced components at C20. (a) High-passed (HP) (filter cutoff period 10 days) wind and current. (b) Low-passed (LP) wind and current. (c) Observed and estimated HP current. (d) Locally and remotely forced LP along-shore current. (e) Locally and remotely forced current (sum of HP and LP local currents). (f) Observed and estimated (sum of locally and remotely forced components) current. Units are dm s^{-1} for wind and cm s^{-1} for current. The abscissa gives the time in Julian Day of 2003. The corresponding figures for the other four current meters are shown in Figures S4–S7. See Figure S8 for a colour version of this figure.

Figure 6. Source of the remote forcing. The top panel shows HP (filter cutoff period 10 days) along-shore winds from QuikSCAT at 15.5°N (grey) and the anemometer (black) at Dona Paula; both QuikSCAT and anemometer winds are in m s^{-1}. The second panel shows the LP (filter cutoff period 10 days) along-shore winds from QuikSCAT at 15.5°N (grey; m s^{-1}) and the anemometer (black; dm s^{-1}) at Dona Paula. The third panel shows the remotely forced current at C20. The bottom panel shows a time-latitude plot of the LP along-shore winds (m s^{-1}) from QuikSCAT. Negative or northwesterly or equatorward (positive or southeasterly or poleward) winds are shown by dashed (solid) contours. The abscissa for all four panels gives the time in Julian Day of 2003. The poleward along-shore wind occurs only south of $\sim$ 9°N, which is roughly the latitude of Kollam (see Figure 1b). The southern limit of this plot is at the southern tip of India ($\sim$ 8°N).

Figure 7. Locally forced (top) and remotely forced (bottom) currents (cm s^{-1}) at the five current meter locations. The black curve is for C20 and the grey curves are for the other four current meters. The abscissa gives the time in Julian Day of 2003. For a summary of the HP and LP observed and estimated components and local and remote components for all five current meters, see Figure S9.

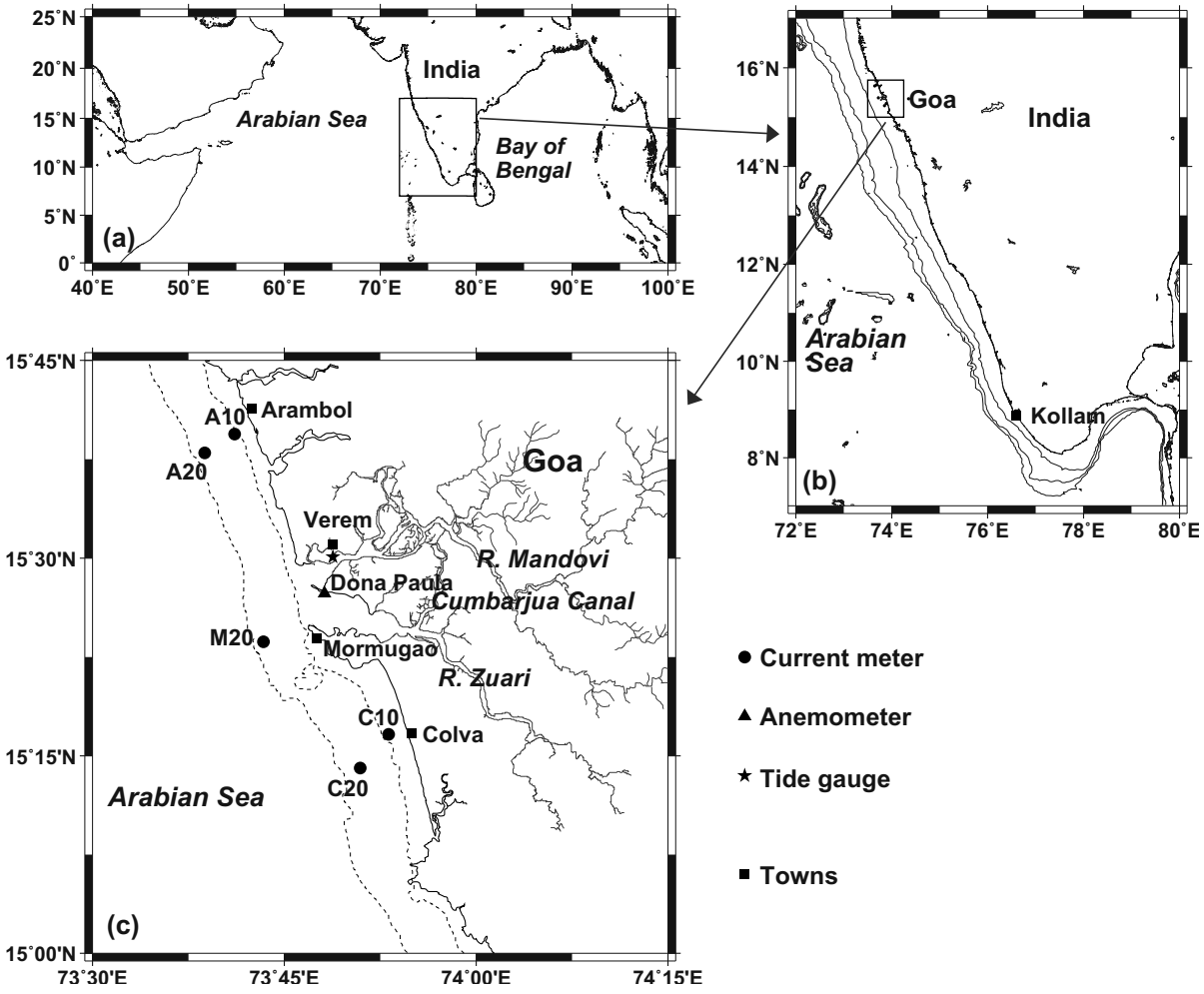
25˚N
20˚N
15˚N
10˚N
5˚N
0˚
40˚E
50˚E
60˚E
70˚E
80˚E
90˚E
100˚E
India
Arabian Sea
Bay of Bengal
(a)
16˚N
14˚N
12˚N
10˚N
8˚N
72˚E
74˚E
76˚E
78˚E
80˚E
Goa
India
Arabian Sea
Kollam
(b)
15˚45'N
15˚30'N
15˚15'N
15˚00'N
73˚30'E
73˚45'E
74˚00'E
74˚15'E
A10
Arambol
A20
Goa
Verem
R. Mandovi
Dona Paula
Cumbarjua Canal
M20
Mormugao
R. Zuari
C10
Colva
C20
Arabian Sea
(c)
Current meter
Anemometer
Tide gauge
Towns

Figure 1

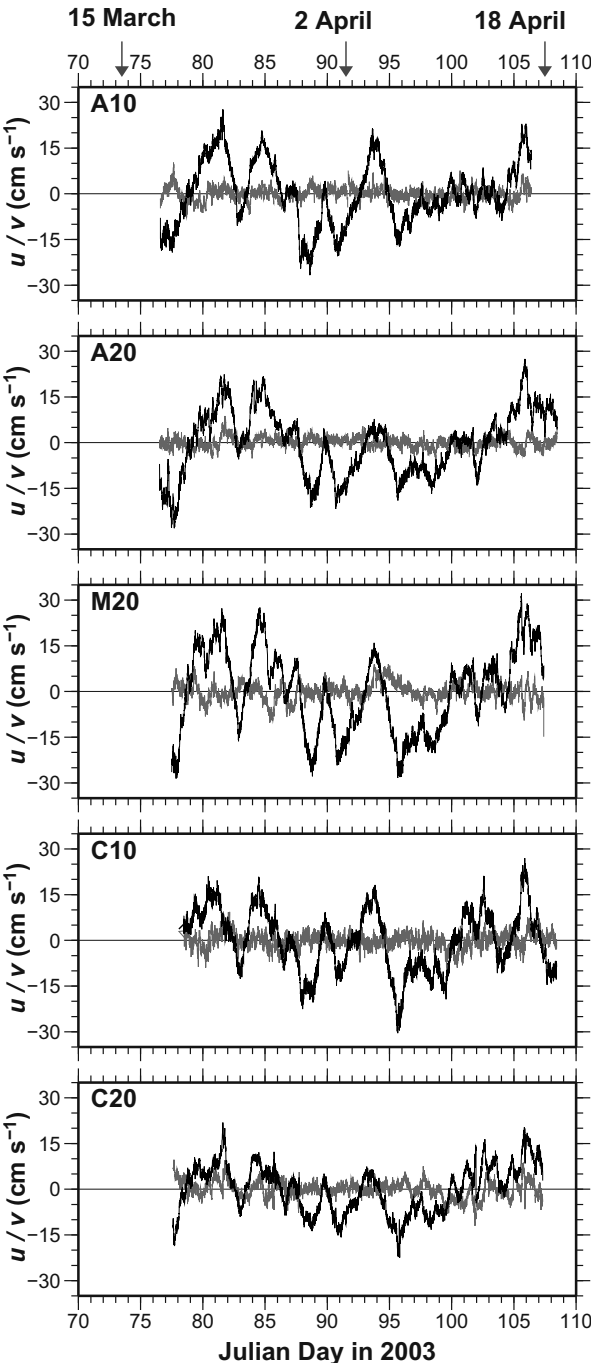
15 March
2 April
18 April
70 75 80 85 90 95 100 105 110
A10
A20
M20
C10
C20
u / v (cm s−1)
30 15 0 −15 −30
Julian Day in 2003

Figure 2

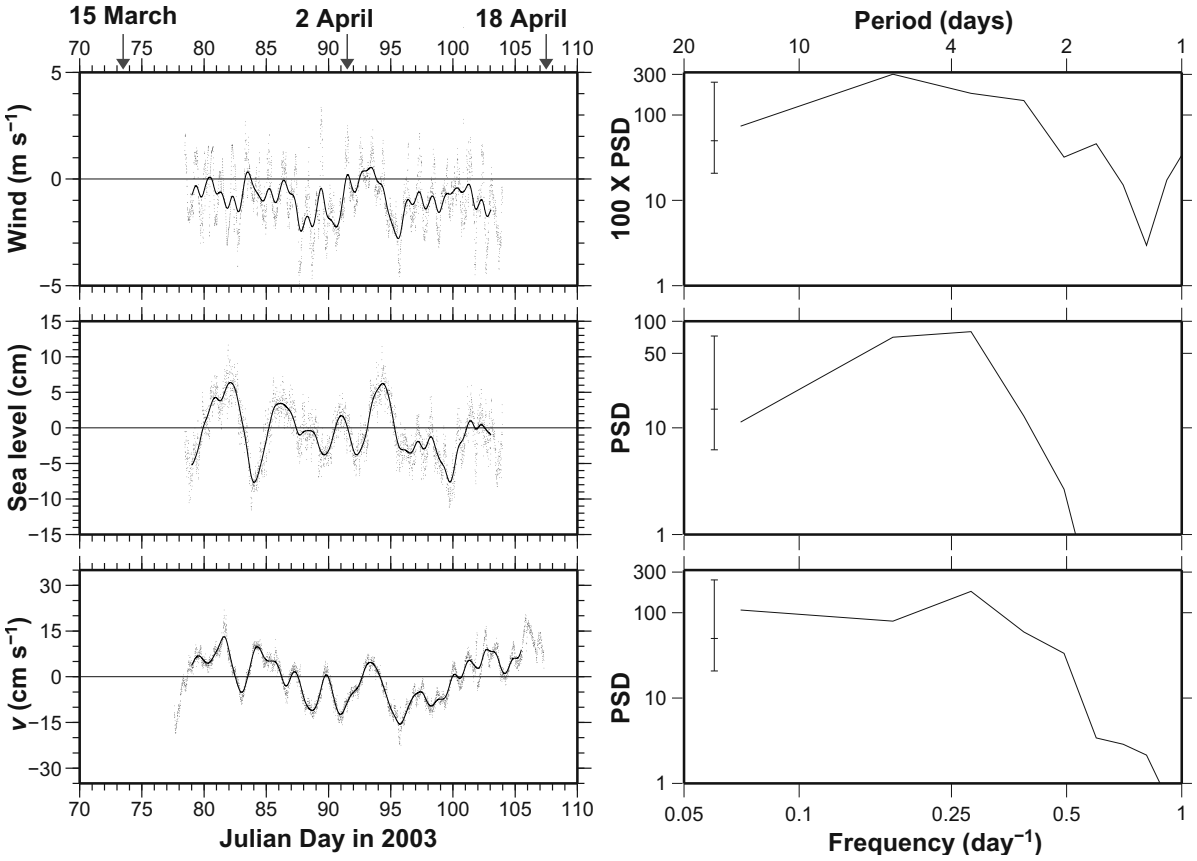
15 March
2 April
18 April
Wind (m s−1)
Sea level (cm)
v (cm s−1)
Julian Day in 2003
Period (days)
100 X PSD
PSD
PSD
Frequency (day−1)

Figure 3

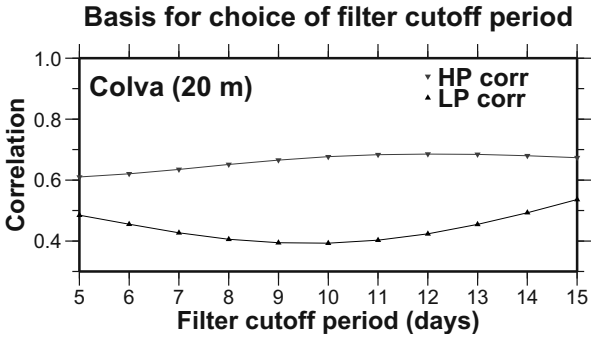
Basis for choice of filter cutoff period
Colva (20 m)
HP corr
LP corr
Correlation
1.0
0.8
0.6
0.4
5
6
7
8
9
10
11
12
13
14
15
Filter cutoff period (days)

Figure 4

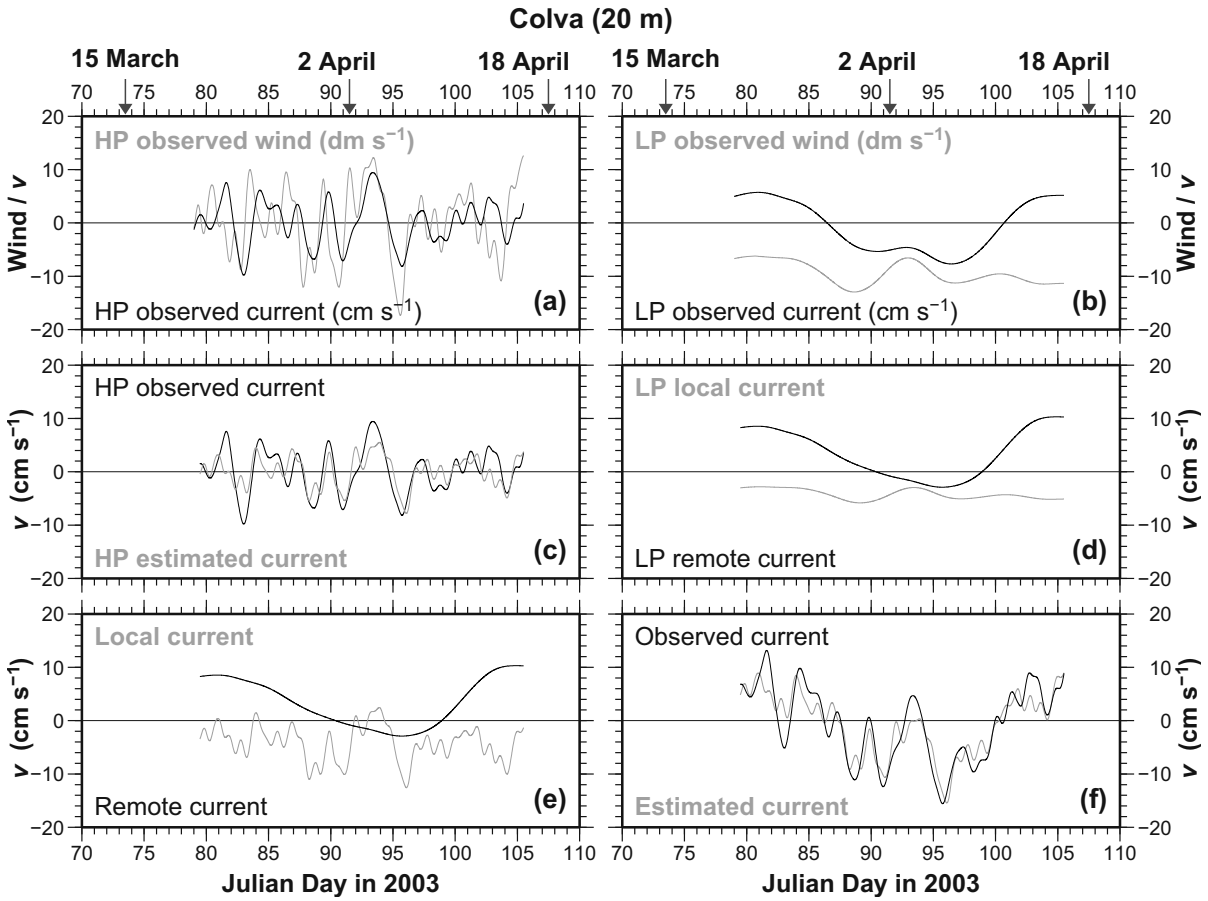
Colva (20 m)
15 March
2 April
18 April
HP observed wind (dm s−1)
HP observed current (cm s−1)
(a)
LP observed wind (dm s−1)
LP observed current (cm s−1)
(b)
Wind / v
HP observed current
HP estimated current
(c)
LP local current
LP remote current
(d)
v (cm s−1)
Local current
Remote current
(e)
Observed current
Estimated current
(f)
Julian Day in 2003

Figure 5

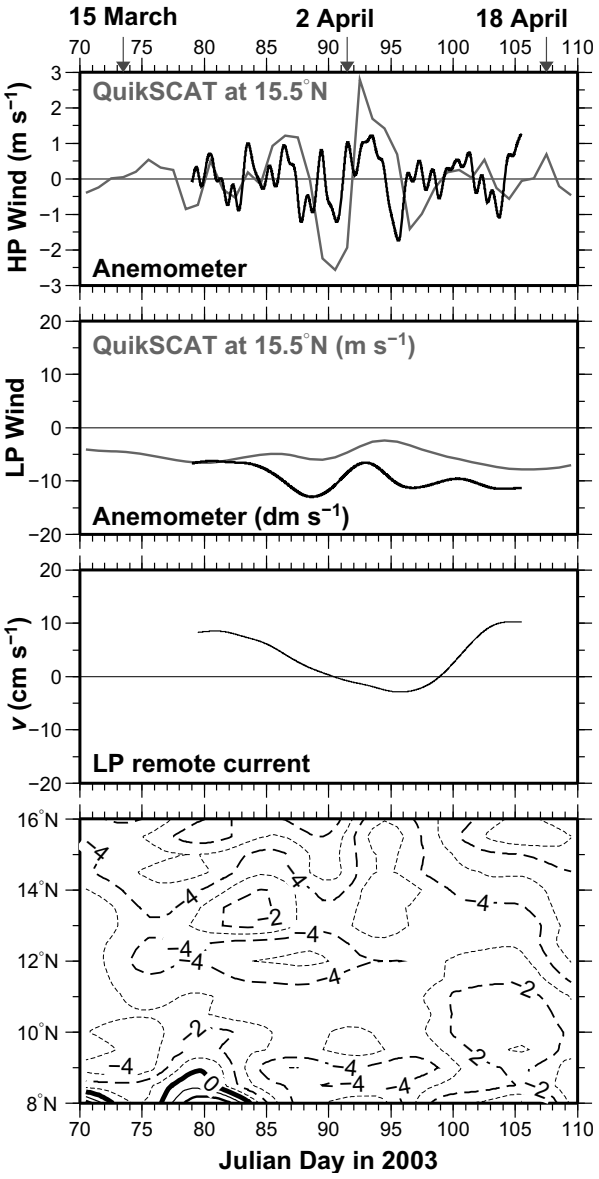
15 March
2 April
18 April
70 75 80 85 90 95 100 105 110
HP Wind (m s−1)
QuikSCAT at 15.5°N
Anemometer
LP Wind
QuikSCAT at 15.5°N (m s−1)
Anemometer (dm s−1)
v (cm s−1)
LP remote current
16°N
14°N
12°N
10°N
8°N
Julian Day in 2003

Figure 6

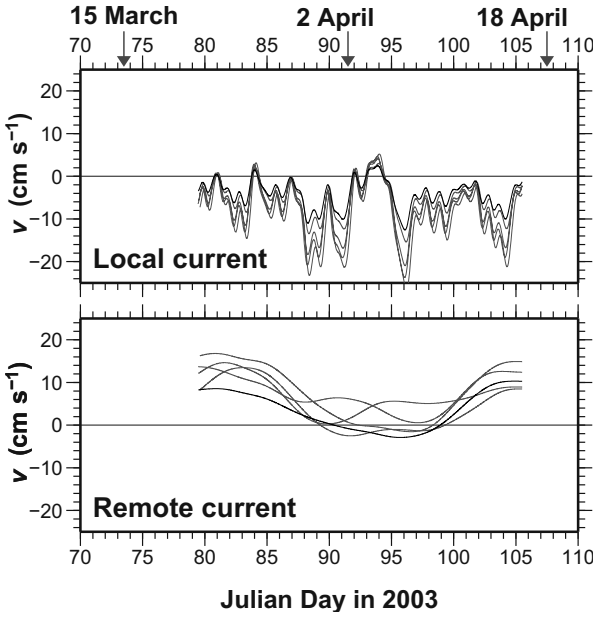
15 March
2 April
18 April
70
75
80
85
90
95
100
105
110
20
10
0
−10
−20
v (cm s−1)
Local current
Remote current
Julian Day in 2003

Figure 7

The auxiliary material consists of nine figures, whose captions are given below. These nine figures are in five files.

1. 2008jc004874-fs01.eps (Figure S1)

Figure S1. (Left) Smoothed periodograms for the five current meters. The bottom panel, for C20, is identical to the bottom right panel in Figure 3; refer to the caption for this figure for details of the periodogram. (Right) Wavelet power spectrum for the five current meters. The bottom panel, for C20, is identical to the bottom right panel in Figure S2; refer to the caption for this figure for details of the wavelet.

2. 2008jc004874-fs02.eps (Figures S2 and S3)

Figure S2. (Left) (Same as left panel of Figure 3.) Along-shore wind (top, m/s), de-tided sea level (middle, cm), and de-tided along-shore current (bottom, cm/s) (grey curves). The current plotted is for current meter C20. The black curves superimposed on the wind, de-tided current, and sea level are the wind, current, and sea level filtered with a 0.75 per day (~ 32 hours) filter that eliminates the sea breeze and its effect. The abscissa gives the time in Julian Day of 2003. (Right) Wavelet power spectrum (plotted on a logarithmic scale to base 2) for wind (top), sea level (middle), and current (bottom); we used the Morlet wavelet for the analysis. The abscissa gives the time in Julian Day of 2003 and the ordinate is the period (in days), which is plotted on a logarithmic scale with base 2. Gray shading has been used to mask wavelet power below the 95% significance level. The solid line shows the cone of influence. The wavelet analysis was performed on the de-tided data using the MATLAB package of Torrence and Compo [1998].

Figure S3. Correlation between wind and along-shore current as a function of filter cutoff period. The HP (high-passed, filter cutoff period on abscissa) correlation (grey curve, inverted triangles) peaked at around 10 days for all five current meters; for most current meters, the LP (low-passed) correlation (black curve, triangles) was a minimum at around 10 days. Hence, a filter cutoff period of 10 days was used to separate the HP component from the LP component.

3. 2008jc004874-fs03.eps (Figures S4 and S5)

Figure S4. Separation of along-shore current into locally and remotely forced components at A10. (a) High-passed (HP) (filter cutoff period 10 days) wind and current. (b) Low-passed (LP) wind and current. (c) Observed and estimated HP current. (d) Locally and remotely forced LP along-shore current. (e) Locally and remotely forced current (sum of HP and LP local currents). (f) Observed and estimated (sum of locally and remotely forced components) current. Units are dm/s for wind and cm/s for current. The abscissa gives the time in Julian Day of 2003. The corresponding figure for C20 is shown in Figure 5 and Figure S8.

Figure S5. As in Figure S4, but for current meter A20.

4. 2008jc004874-fs04.eps (Figures S6 and S7)

Figure S6. As in Figure S4, but for current meter M20.

Figure S7. As in Figure S4, but for current meter C10.

5. 2008jc004874-fs05.eps (Figures S8 and S9)

Figure S8. As in Figure S4, but for current meter C20. This figure is a colour version of Figure 5.

Figure S9. Summary of the analysis for all five current meters. (a) HP observed current (compare with the black curves in Figure 5a,c). (b) HP estimated current (compare with the grey curve in Figure 5c). (c) LP observed current (compare with the black curve in Figure 5b). (d) LP estimated current (compare with the sum of the LP local and remote components shown in Figure 5d). (e) Local component of the current (compare with the grey curve in Figure 5e). (f) Remote component of the current (compare with the black curve in Figure 5e). The black (grey) curves are for current meter C20 (C10), the green (red) curves for A20 (A10), and the blue curves for M20. The local (e) and remote (f) components of the current for all five current meters are also shown in Figure 7. The abscissa gives the time in Julian Day of 2003.

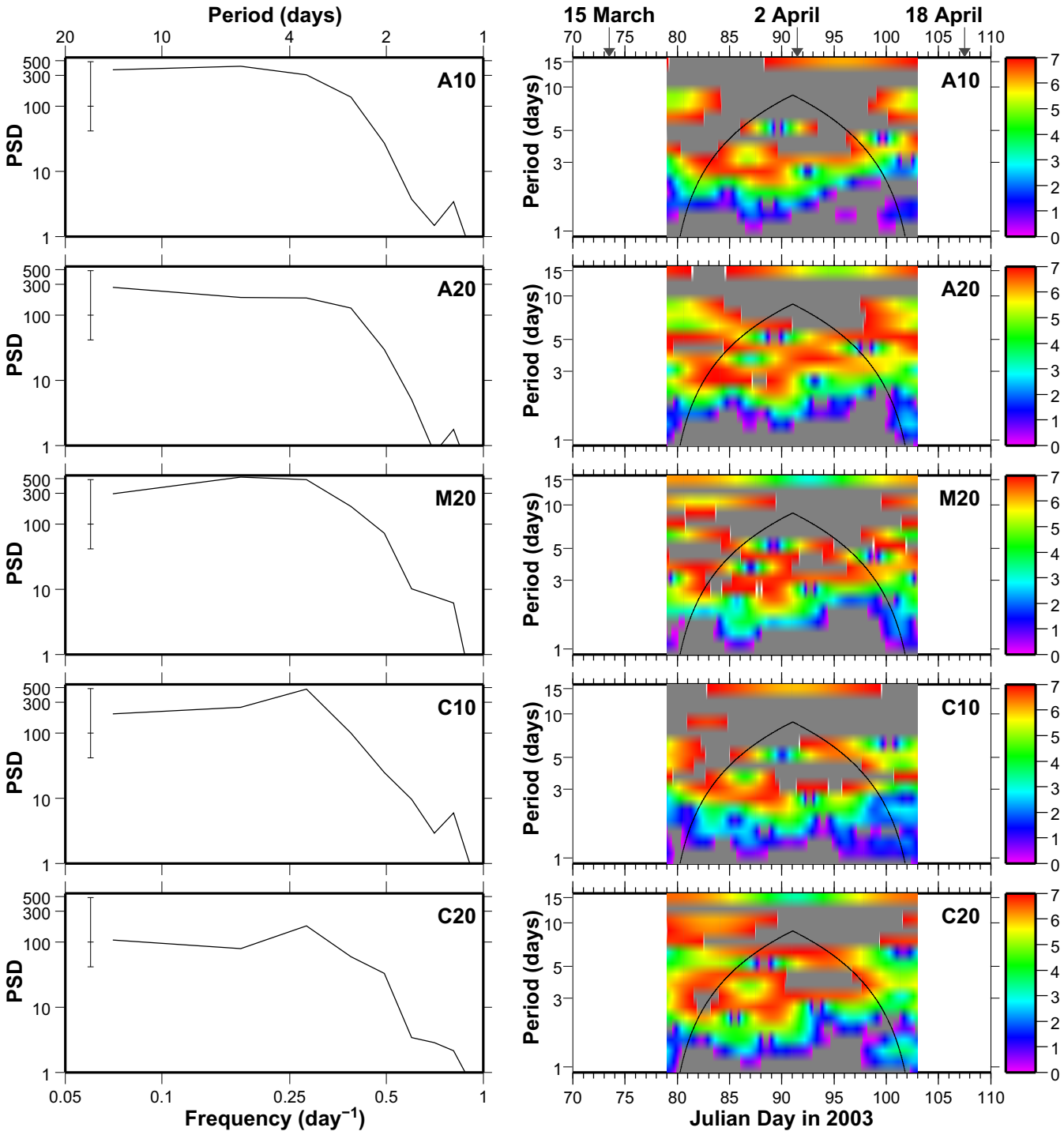
Period (days)
20
10
4
2
1
PSD
500
300
100
10
1
A10
A20
M20
C10
C20
0.05
0.1
0.25
0.5
1
Frequency (day^{-1})
15 March
2 April
18 April
70
75
80
85
90
95
100
105
110
Period (days)
15
10
5
3
1
7
6
5
4
3
2
1
0
Julian Day in 2003

Figure S1

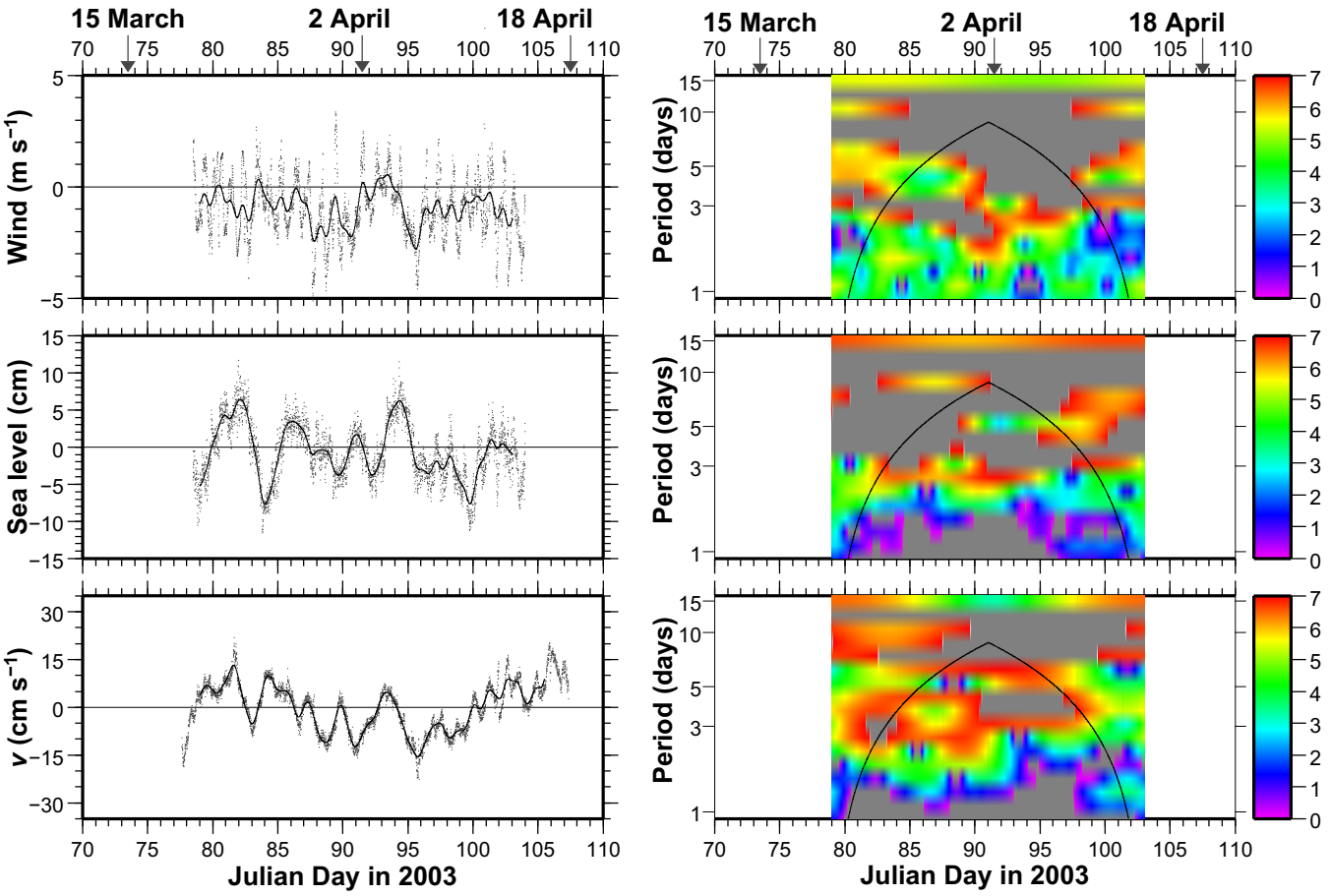

Figure S2

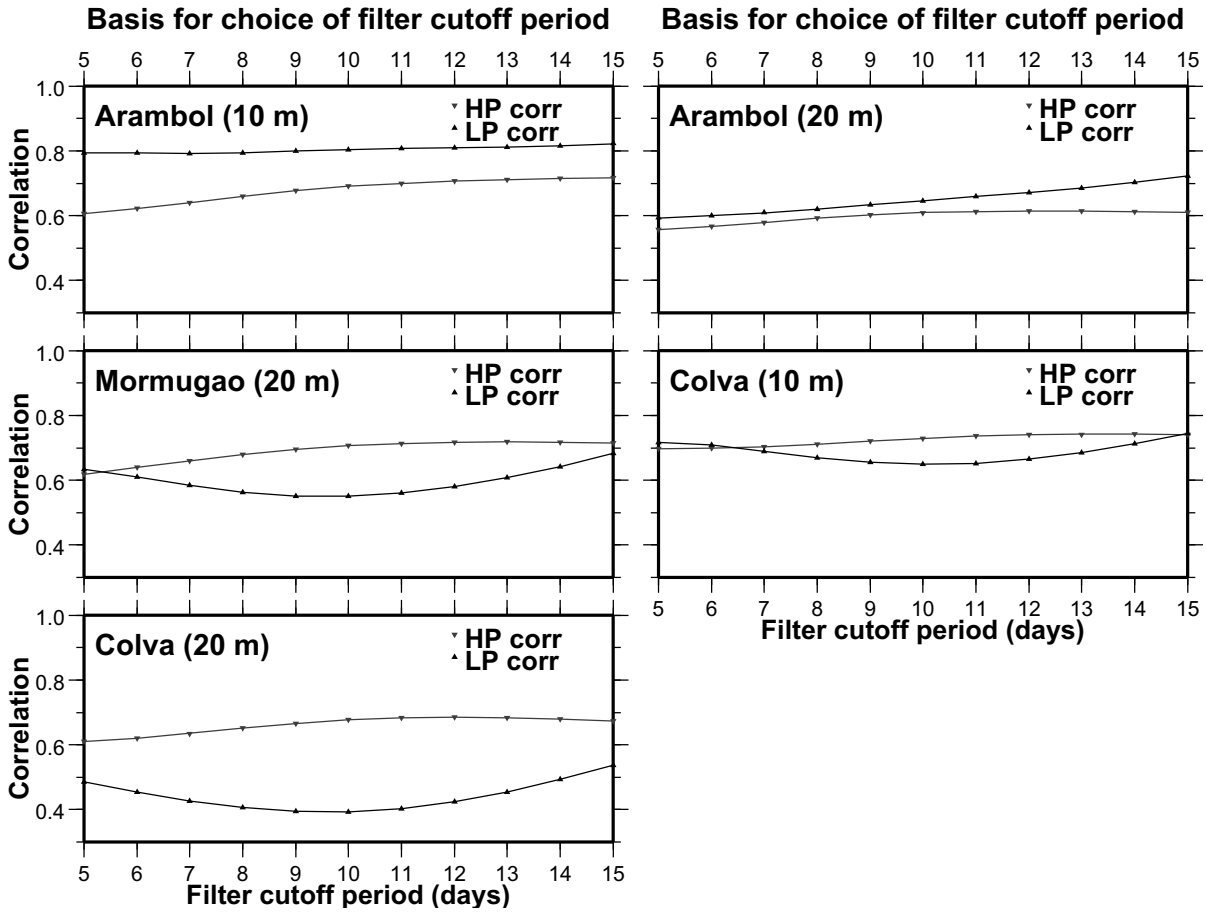

Figure S3

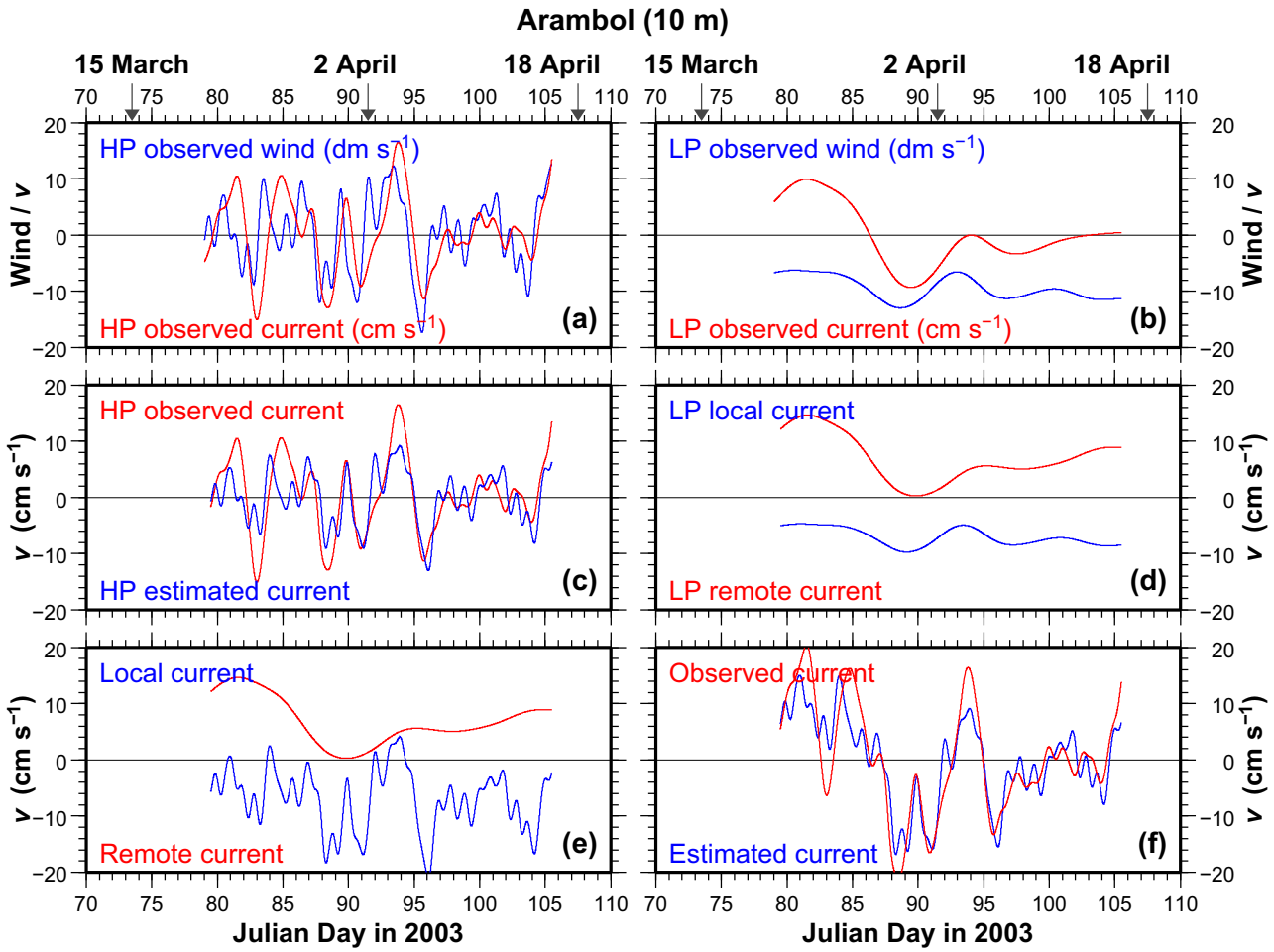

Figure S4

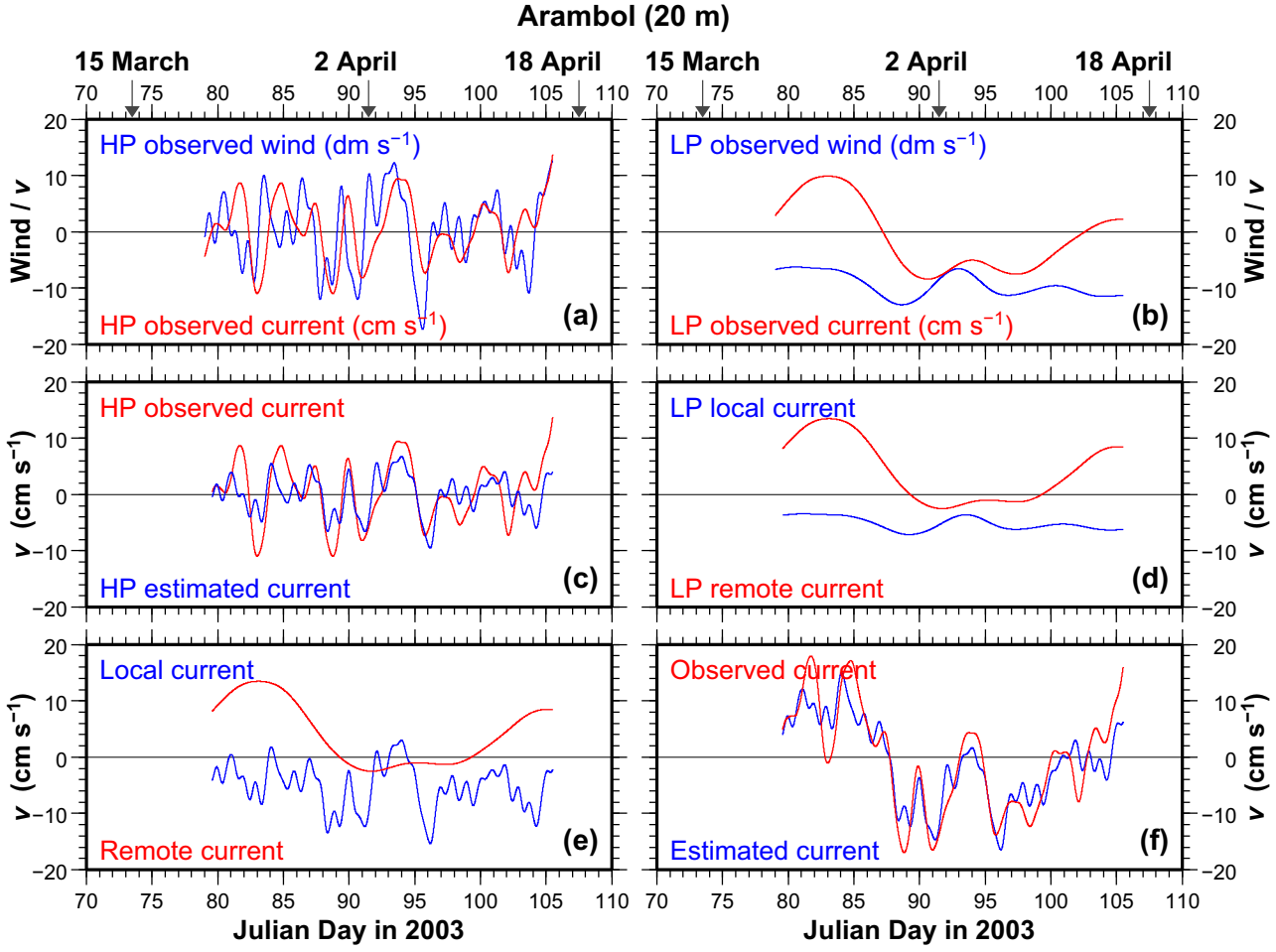

Figure S5

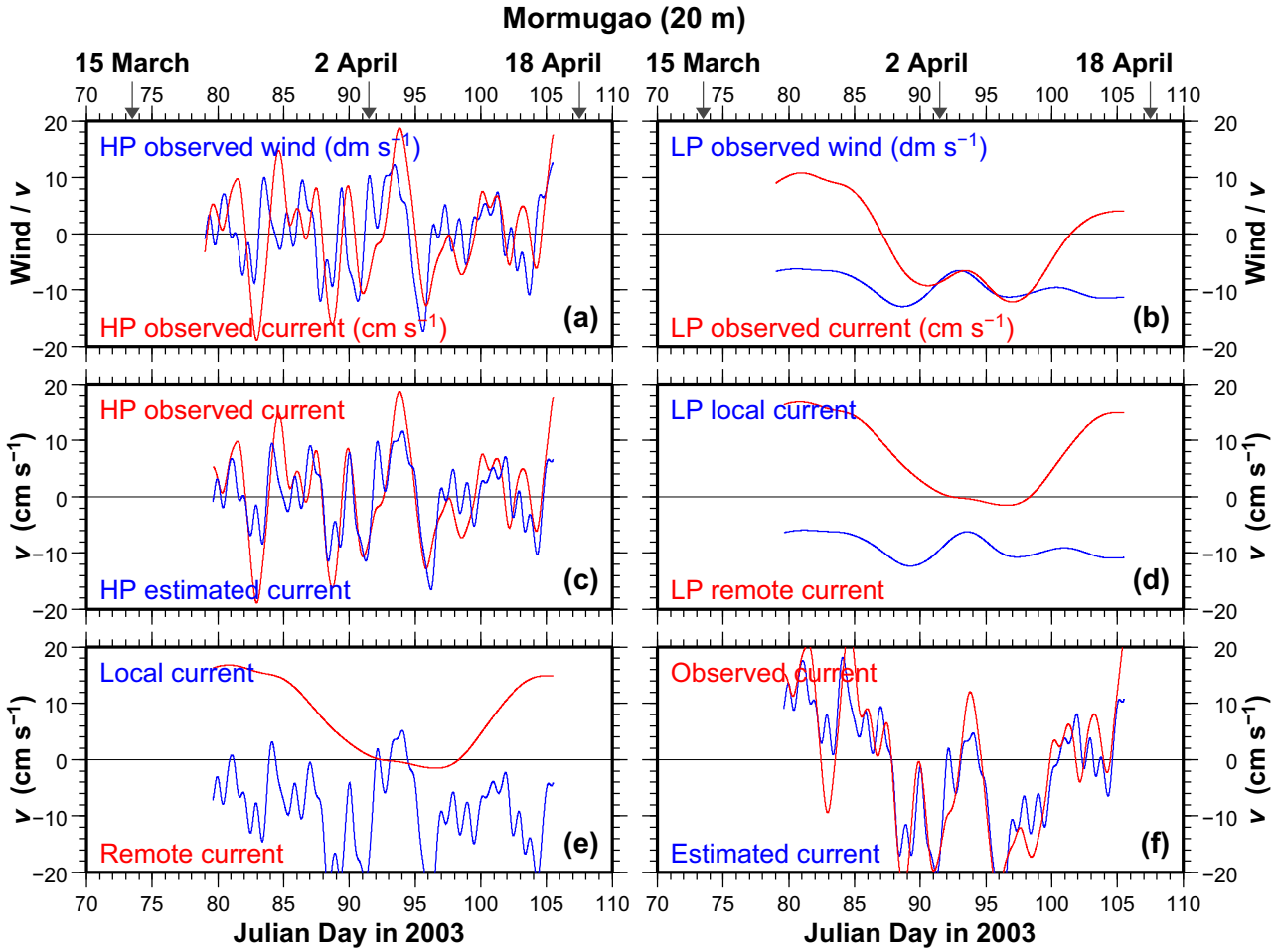

Figure S6

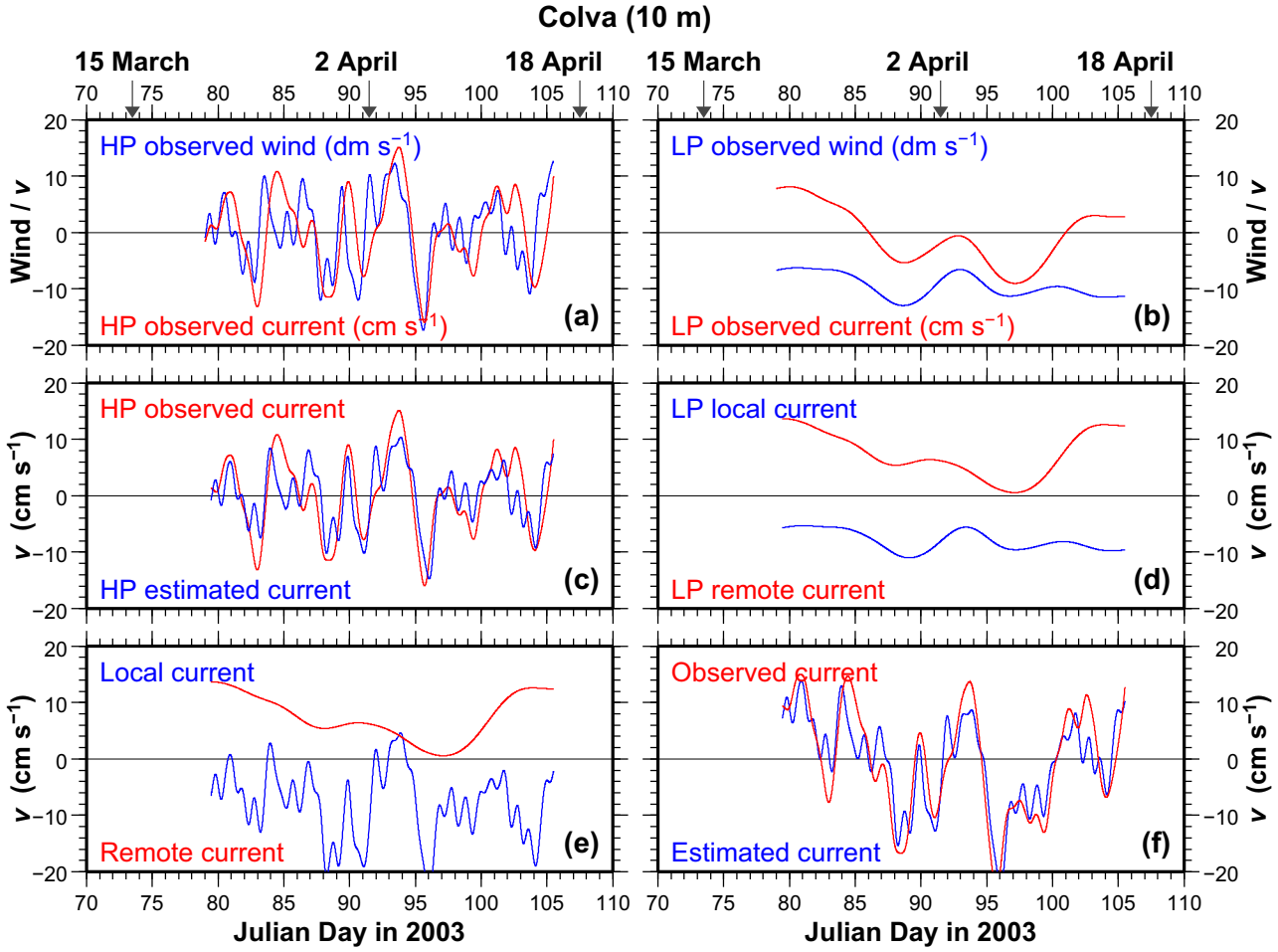

Figure S7

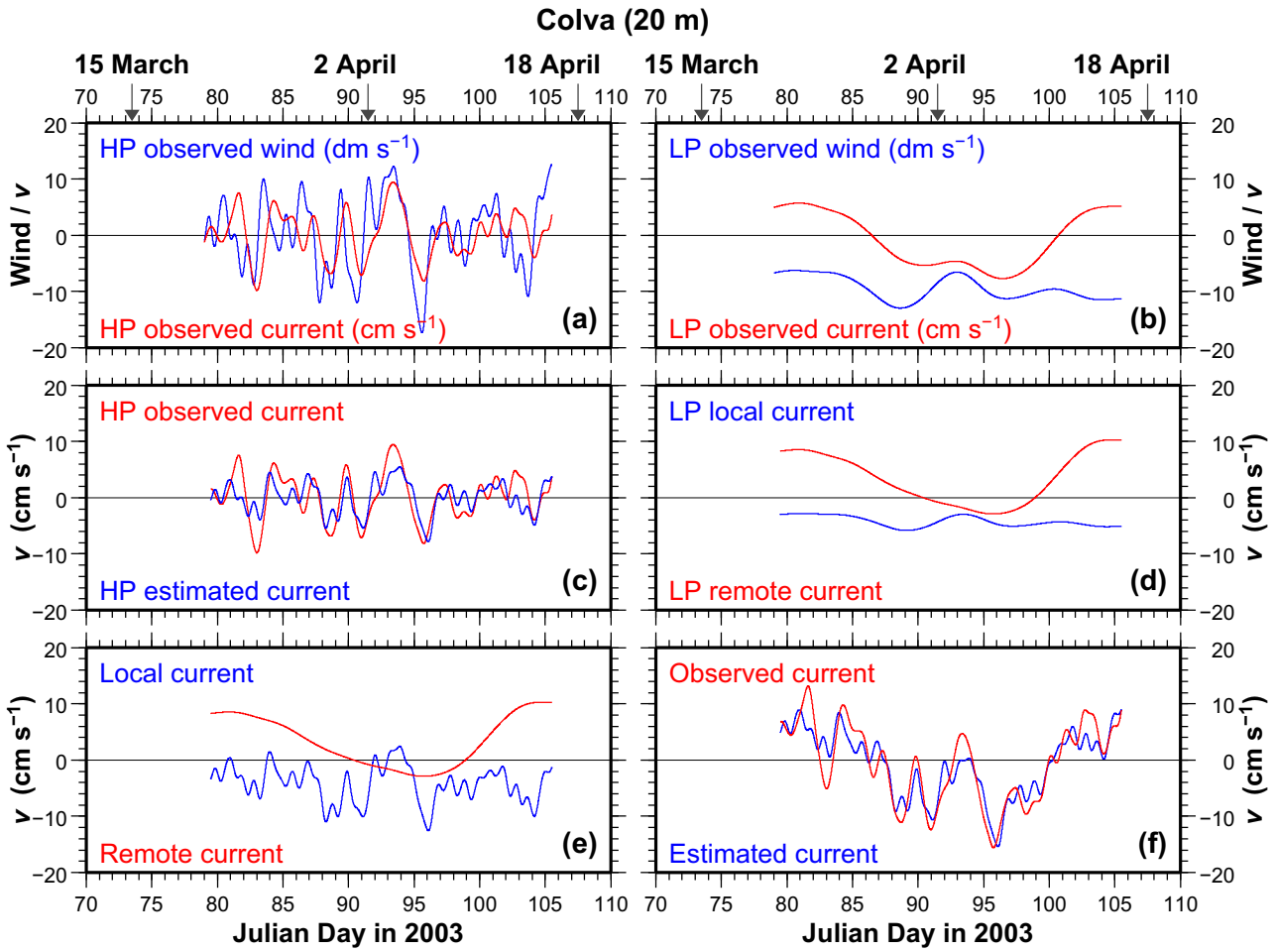

Figure S8

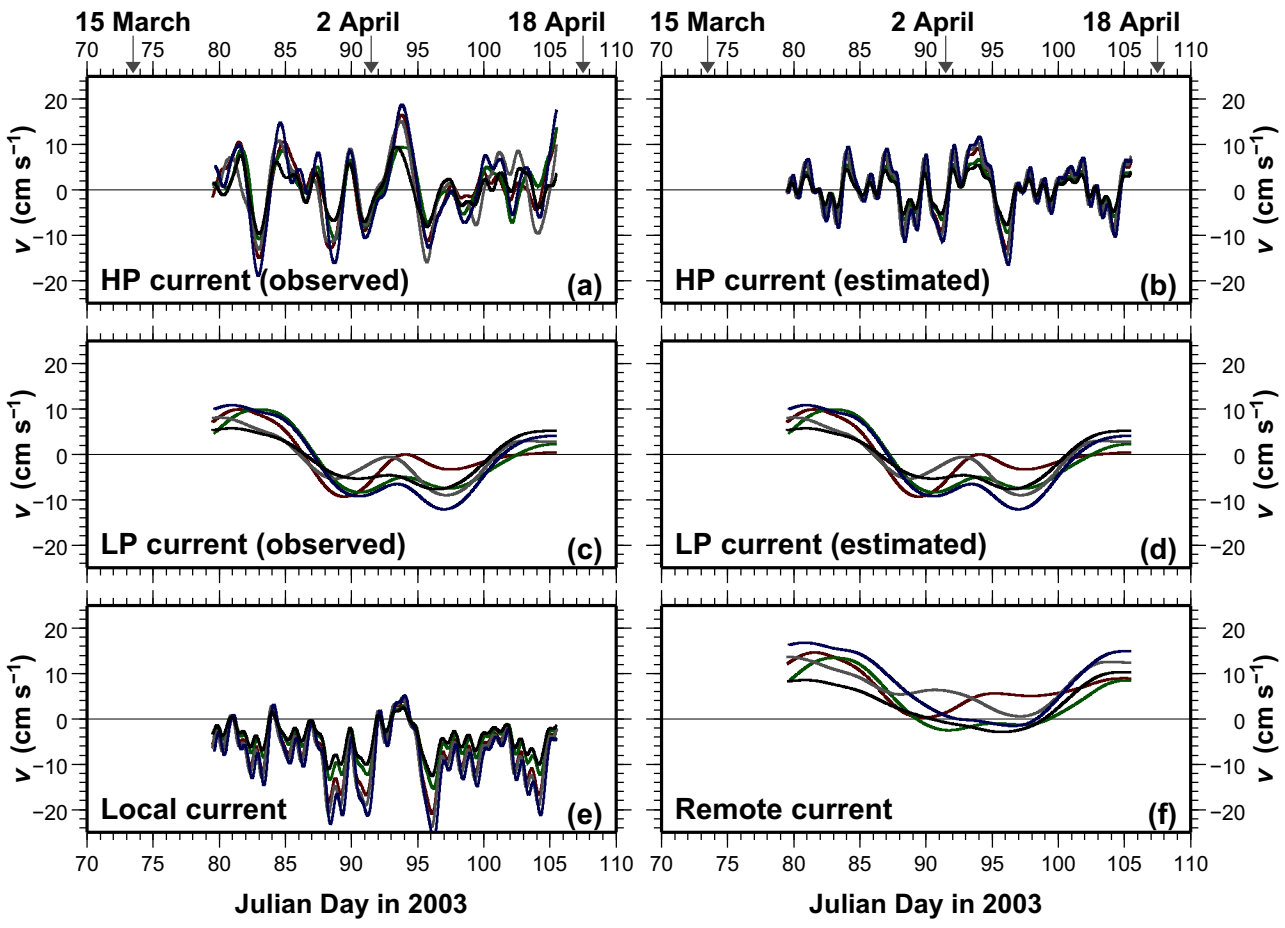

Figure S9